nature astronomy

SUPPLEMENTARY INFORMATION

https://doi.org/10.1038/s41550-018-0568-z

In the format provided by the authors and unedited.

A UV resonance line echo from a shell around a hydrogen-poor superluminous supernova

R. Lunnan[1,2*], C. Fransson[1], P. M. Vreeswijk[3], S. E. Woosley[4], G. Leloudas[5], D. A. Perley[6], R. M. Quimby[7,8], Lin Yan[9], N. Blagorodnova[2], B. D. Bue[10], S. B. Cenko[11,12], A. De Cia[13], D. O. Cook[2], C. U. Fremling[2], P. Gatkine[11], A. Gal-Yam[3], M. M. Kasliwal[2], S. R. Kulkarni[2], F. J. Masci[14], P. E. Nugent[15,16], A. Nyholm[1], A. Rubin[3], N. Suzuki[8] and P. Wozniak[17]

[1]Oskar Klein Centre, Department of Astronomy, Stockholm University, Stockholm, Sweden. [2]Department of Astronomy, California Institute of Technology, Pasadena, CA, USA. [3]Benoziyo Center for Astrophysics and the Helen Kimmel Center for Planetary Science, Weizmann Institute of Science, Rehovot, Israel. [4]Department of Astronomy and Astrophysics, University of California, Santa Cruz, CA, USA. [5]Dark Cosmology Centre, Niels Bohr Institute, University of Copenhagen, Copenhagen, Denmark. [6]Astrophysics Research Institute, Liverpool John Moores University, Liverpool, UK. [7]Department of Astronomy, San Diego State University, San Diego, CA, USA. [8]Kavli IPMU (WPI), UTIAS, The University of Tokyo, Kashiwa, Chiba, Japan. [9]Caltech Optical Observatories & Infrared Processing and Analysis Center, California Institute of Technology, Pasadena, CA, USA. [10]Jet Propulsion Laboratory, California Institute of Technology, Pasadena, CA, USA. [11]Astrophysics Science Division, NASA Goddard Space Flight Center, Greenbelt, MD, USA. [12]Joint Space-Science Institute, University of Maryland, College Park, MD, USA. [13]European Southern Observatory, Garching bei Munchen, Germany. [14]Infrared Processing and Analysis Center, California Institute of Technology, Pasadena, CA, USA. [15]Lawrence Berkeley National Laboratory, Berkeley, CA, USA. [16]Department of Astronomy, University of California, Berkeley, CA, USA. [17]Los Alamos National Laboratory, MS-D466, Los Alamos, NM, USA. *e-mail: ragnhild.lunnan@astro.su.se

Supplementary Information

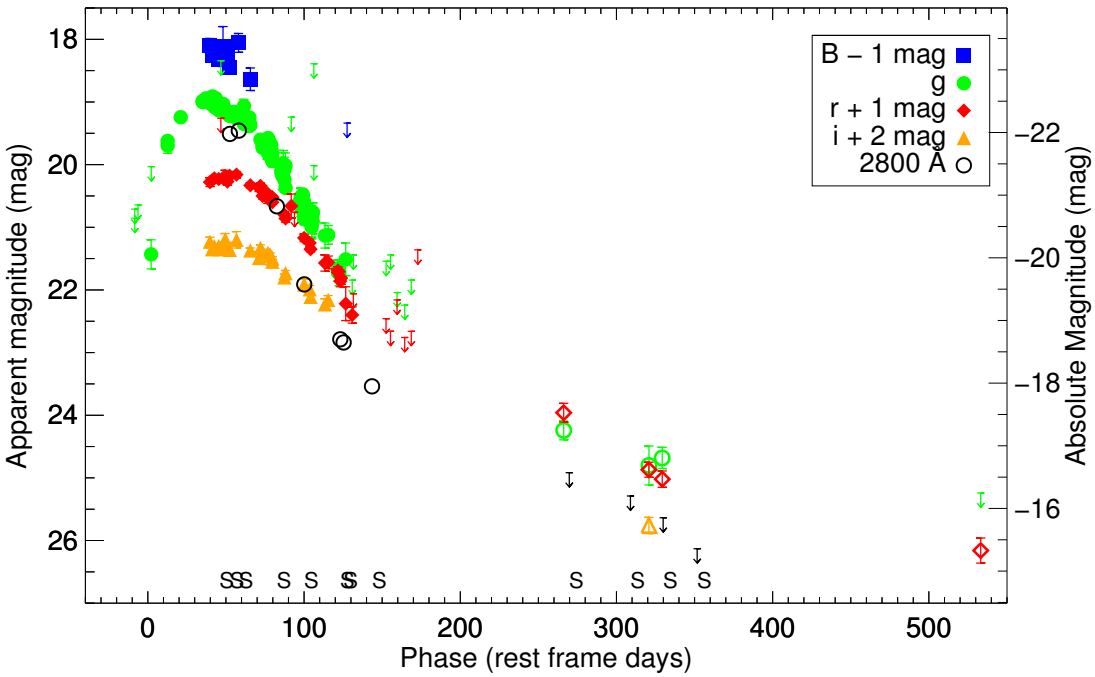

Supplementary Figure 1 Observed light curve of iPTF16eh. Data is mainly from the P48 and P60 telescopes, and is listed in Supplementary Table 1. Filters have been offset for clarity as indicated in the legend, and dates of the spectroscopy epochs are marked with S symbols along the bottom axis. Upper limits are 5σ. The open symbols after 200 days show unsubtracted photometry, and may have a significant host galaxy contribution. Open black circles show the flux at a rest-frame wavelength of 2800 Å, as measured from the continuum flux in the spectra in the region 2765 – 2834 Å.

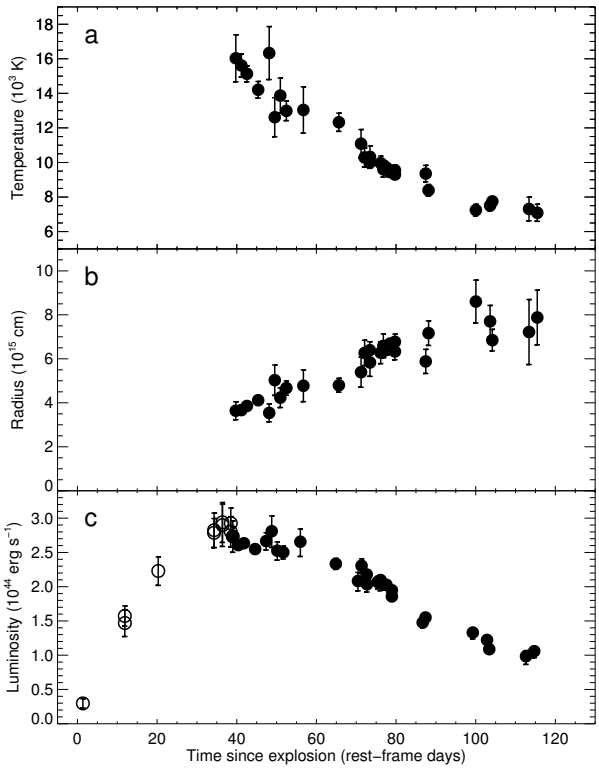

Supplementary Figure 2 Evolution of (a) the blackbody temperature, (b) the blackbody radius, and (c) the pseudo-bolometric luminosity. Blackbody parameters are derived by fitting a Planck function to the observed photometry using IDL's `mpfit` routine, and the error bars plotted are the 1σ uncertainties given the observed photometry. The pseudo-bolometric luminosity is calculated by integrating the observed flux as well as a blackbody tail redwards of the observed bands, and the plotted uncertainties include both these components. As we do not have multiband data on the rise of the light curve, the points on the rise are calculated scaling from the g-band light curve and assuming a constant bolometric correction (open circles). Any extra (systematic) uncertainty from this assumption is not included in the error bars, which reflect the statistical uncertainties only.

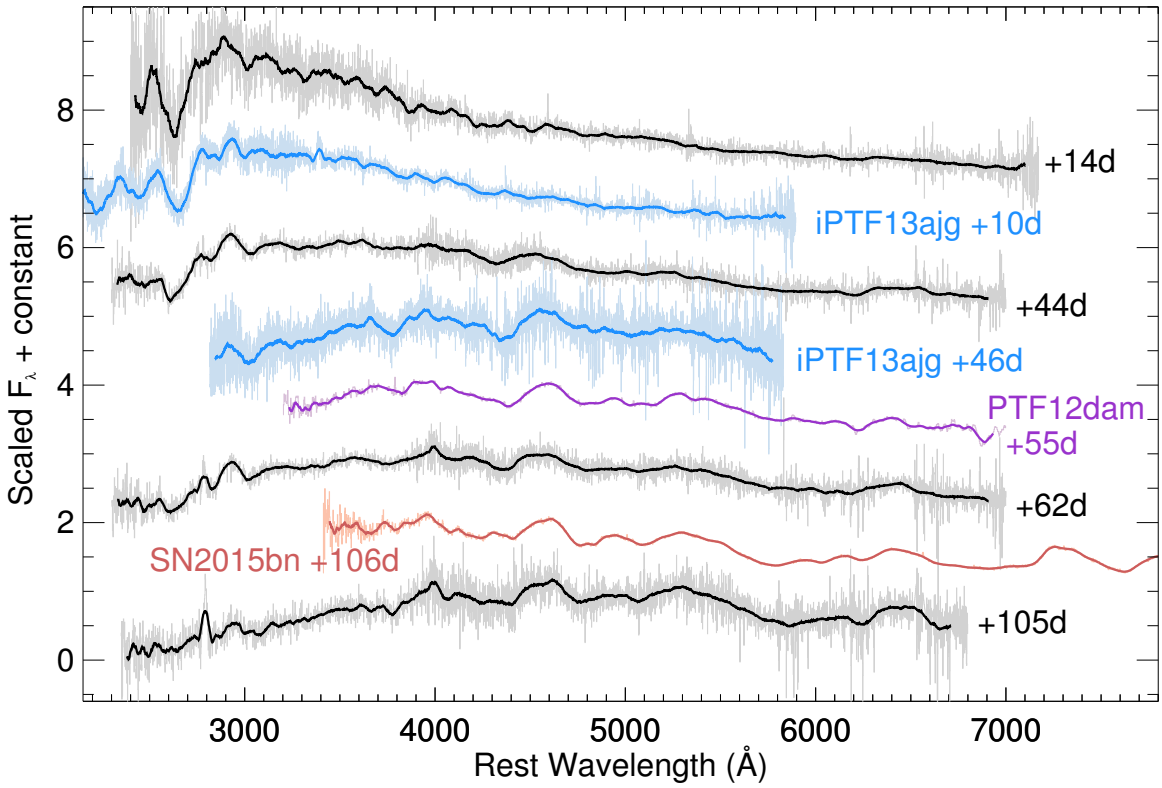

Supplementary Figure 3 Spectra of iPTF16eh (black) compared to the well-studied SLSNe PTF12dam[?], iPTF13ajg[?], and SN 2015bn[?]. To facilitate comparisons, supernova phases are labeled relative to peak light (MJD 57424.3 in the case of iPTF16eh). The spectra are smoothed by a Savitzky-Golay filter, with the unsmoothed data shown in the background. The spectra have been normalized to the flux level at 4000 Å and are offset from each other by one scale unit.

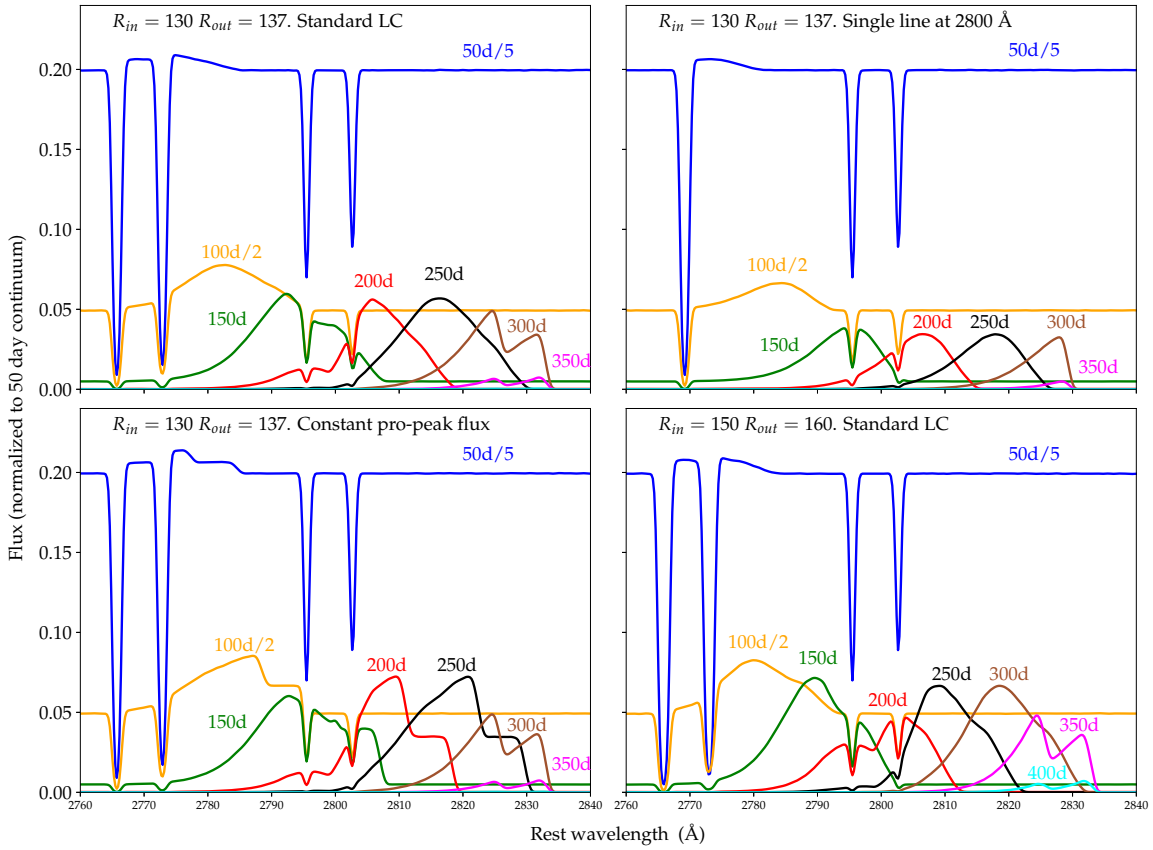

Supplementary Figure 4 Time sequence of simulated spectra in the Mg II wavelength region, similar to Figure 3 of the main article, for different choices of shell parameters and input light curves. *Upper left:* Standard values for the light curve and shell, $R_{\rm in} = 130$ light days, $R_{\rm in} = 137$ light days. *Upper right:* Same parameters, but with only a single line at a rest wavelength 2800 Å. Note the double-peaked line profiles, the broader lines, as well as the nearly double intensity in the doublet case. *Lower left:* Same shell parameters, but constant continuum flux before the peak. Note the flat red plateau in the line profile. *Lower right:* Effect of changing the parameters of the shell to $R_{\rm in} = 150$ light days, $R_{\rm in} = 160$ light days. Standard light curve. Note the slower evolution in wavelength and narrower line profiles. No smoothing due to the instrumental resolution has been applied too these simulations.

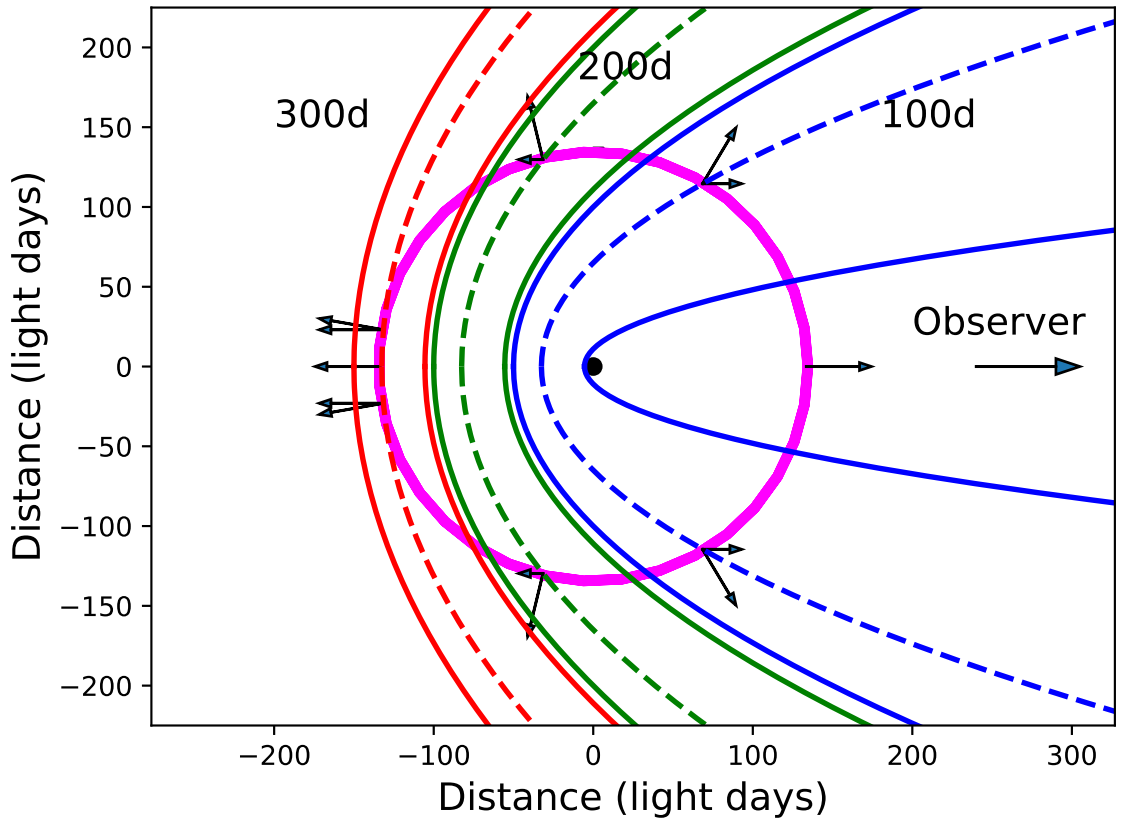

Supplementary Figure 5 Approximate geometry of the shell and light echo parabolas, corresponding to three different observed epochs, 100, 200 and 300 days after explosion. The outer parabola corresponds to the shock breakout and the dashed to the peak luminosity, assumed to be at ~ 35 days after shock breakout. The inner parabola, representing the end of the light curve, is defined by the time after shock breakout corresponding to 95% of the integrated luminosity of the model light curve, here 89 days. The radial and horizontal arrows correspond to the expansion velocity of the ring, ~ 3300 km s^{-1}, and the line of sight velocity for the peak of the light curve, respectively.

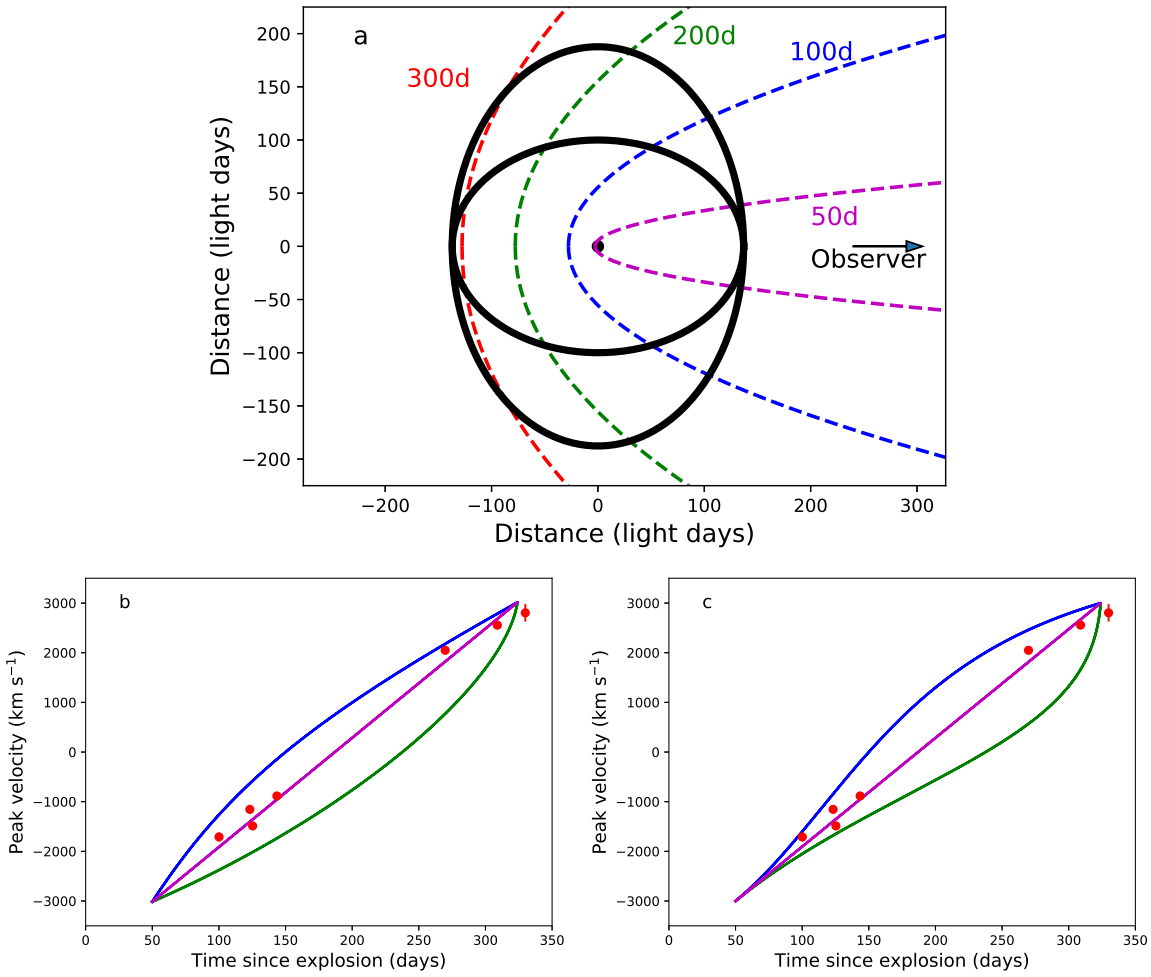

Supplementary Figure 6 Panel a: Same as Fig. 5 but for two additional shell geometries, with ellipsoids with major (minor) axis 137 light days along the line of sight and minor (major) axis perpendicular to the line of sight and an axial ratio of 1.37. See text for details. Panels b and c: Peak velocity evolution for these geometries for a shell with $V \propto r$ (Panel b) and V =constant (Panel c). The purple line shows the spherical case, the blue line the ellipsoid with major axis 137 light days, and the green line the ellipsoid with minor axis 137 light days. Note the departures from the linear evolution in all of the non-spherical cases.

Supplementary Table 1. iPTF16eh Photometry

MJD (days)	Rest-frame Phase (days)	Filter	AB Mag	Instrument
57358.53	-8.39	g	> 20.71	P48
57358.56	-8.37	g	> 20.86	P48
57361.54	-6.28	g	> 20.64	P48
57373.54	2.13	g	21.43 ± 0.23	P48
57373.57	2.15	g	> 20.03	P48
57388.55	12.65	g	19.62 ± 0.07	P48
57388.58	12.67	g	19.70 ± 0.12	P48
57400.55	21.06	g	19.24 ± 0.07	P48
57420.53	35.05	g	19.00 ± 0.03	P48
57420.56	35.08	g	18.99 ± 0.06	P48

Note. — Full table is available as a separate, machine-readable file. A portion is shown here for clarity.

Supplementary Table 2. Summary of Spectroscopic Observations

Observation Date (YYYY MM DD.D)	Phase[a] (rest-frame days)	Telescope+Instrument	Grating[b]	Exp. time[b] (s)	Airmass
2016 Feb 18.5	45.9	Subaru+FOCAS	···	600	1.03
2016 Feb 27.5	52.5	P200+DBSP	600/4000, 316/7500	900	1.16
2016 Mar 06.6	58.2	Keck I+LRIS	400/3400, 400/8500	280, 240	1.27
2016 Apr 10.3	82.5	Keck I+LRIS	400/3400, 400/8500	300, 300	1.11
2016 May 05.4	100.1	Keck I+LRIS	400/3400, 400/8500	1200, 1120	1.16
2016 Jun 07.3	123.2	Keck I+LRIS	400/3400, 400/8500	600, 520	1.18
2016 Jun 10.4	125.3	Keck I+LRIS	600/4000, 400/8500	1905, 1800	1.55
2016 Jul 06.3	143.5	Keck I+LRIS	400/3400, 400/8500	2400, 2280	1.64
2017 Jan 02.6	269.8	Keck I+LRIS	400/3400, 400/8500	2730, 2550	1.26
2017 Feb 27.5	309.0	Keck I+LRIS	400/3400, 400/8500	3600, 3510	1.06
2017 Mar 29.4	329.9	Keck I+LRIS	400/3400, 400/8500	5415, 5070	1.09
2017 Apr 29.4	351.7	Keck I+LRIS	400/3400, 400/8500	7200, 7020	1.25

[a]Relative to best-fit explosion date on 2015 December 14.5. To get phase relative to g-band peak, subtract 37.7 days.

[b]Comma-separated values indicate setup for blue and red arms, respectively.

Supplementary Table 3. Emission Line Properties

MJD (days)	Time since explosion (rest-frame days)	Line centroid (Å , rest-frame)	Line FWHM (Å , rest-frame)	Line flux (10^{-16} erg s^{-1} cm^{-2})
57513.4	100.1	2785.41 ± 0.85	13.7 ± 2.0	1.89 ± 0.37
57546.3	123.2	2790.59 ± 0.76	15.7 ± 1.8	1.42 ± 0.22
57549.4	125.3	2787.48 ± 0.73	12.0 ± 1.7	1.17 ± 0.23
57575.3	143.5	2793.11 ± 0.67	16.6 ± 1.5	1.24 ± 0.16
57755.6	269.8	2820.50 ± 0.24	13.7 ± 0.6	2.02 ± 0.11
57811.5	309.0	2825.24 ± 0.29	12.5 ± 0.7	1.03 ± 0.07
57841.4	329.9	2827.56 ± 1.64	14.4 ± 4.0	0.49 ± 0.17
57872.4	351.7	···	···	< 0.28

Note. — Table is also available in machine-readable form.

Supplementary Table 4. Blackbody Parameters and Pseudo-Bolometric Light Curve

MJD (days)	Time since explosion (rest-frame days)	Pseudo-bolometric luminosity (10^{44} erg s^{-1})	Blackbody temperature (10^3 K	Blackbody radius (10^{15} cm)
57427.3	39.8	2.73 ± 0.14	16.0 ± 1.4	3.6 ± 0.4
57429.2	41.2	2.61 ± 0.07	15.6 ± 0.7	3.7 ± 0.2
57431.2	42.6	2.63 ± 0.05	15.1 ± 0.5	3.9 ± 0.2
57435.3	45.4	2.55 ± 0.07	14.2 ± 0.5	4.1 ± 0.2
57439.2	48.1	2.67 ± 0.13	16.3 ± 1.5	3.5 ± 0.4
57441.2	49.5	2.81 ± 0.23	12.6 ± 1.1	5.0 ± 0.7
57443.2	50.9	2.53 ± 0.13	13.9 ± 1.0	4.2 ± 0.4
57445.4	52.5	2.50 ± 0.09	13.0 ± 0.6	4.7 ± 0.3
57451.5	56.7	2.66 ± 0.20	13.0 ± 1.3	4.8 ± 0.7
57464.2	65.6	2.33 ± 0.08	12.3 ± 0.5	4.8 ± 0.3

Note. — Full table is available as a separate, machine-readable file. A portion is shown here for clarity.